

Uncertainty in AI-driven Monte Carlo simulations

Dimitrios Tzivraïlis^{1,2}, Alberto Rosso², Eiji Kawasaki¹

¹ *Université Paris-Saclay, CEA, List, F-91120 Palaiseau Cedex, France and*

² *LPTMS, CNRS, Université Paris-Saclay, 91405 Orsay, France*

(Dated: June 20, 2025)

In the study of complex systems, evaluating physical observables often requires sampling representative configurations via Monte Carlo techniques. These methods rely on repeated evaluations of the system’s energy and force fields, which can become computationally expensive, particularly in the presence of long-range interactions. To accelerate these simulations, deep learning models are increasingly employed as surrogate functions to approximate the energy landscape or force fields. However, such models introduce epistemic uncertainty in their predictions, which may propagate through the sampling process and affect the system’s macroscopic behavior. In this work, we present the Penalty Ensemble Method (PEM) to quantify epistemic uncertainty and mitigate its impact on Monte Carlo sampling. Our approach introduces an uncertainty-aware modification of the Metropolis acceptance rule, which increases the rejection probability in regions of high uncertainty, thereby enhancing the reliability of the simulation outcomes.

I. INTRODUCTION

The integration of artificial intelligence (AI), particularly machine learning, into scientific methodologies is transforming physics and chemistry. This synergy offers new paradigms for modeling complex phenomena, combining established physical laws with data-driven approaches [1, 2]. However, such powerful data-driven models inherently introduce epistemic uncertainty into their predictions [3].

The investigation of complex systems often necessitates sampling configurations via Monte Carlo techniques, which depend on computationally intensive energy and force field evaluations [4]. To accelerate these simulations and enable studies of larger, intricate systems, deep learning models are increasingly used as efficient surrogate functions [5]. This integration promises to significantly enhance physical modeling by replacing resource-intensive computations with rapid approximations [6].

However, this hybridization introduces significant challenges. Machine learning models yield predictions with statistical properties distinct from those of direct physical calculations, containing inherent “noise” due to the finite and often limited observational data used for training. To effectively characterize these AI models as statistical estimators, robust methods for uncertainty quantification are essential, an area that has begun to be explored [7, 8]. Nevertheless, AI models such as Neural Network Interatomic Potentials (NNIPs) are known to produce unstable simulations, frequently leading to irreversible entry into unphysical regions of phase space [9]. This propagation of predictive noise and the resulting incompatibility of proposed configurations with the simulation, especially as system size increases, represents a major bottleneck for the robust application of deep learning in scientific computing [10]. Such perturbations can profoundly affect the macroscopic behavior of complex, stochastic systems.

This study directly addresses the fundamental challenge of epistemic uncertainty arising from the integra-

tion of deep learning models into physical simulations. When a computationally expensive physical energy calculation is approximated by a neural network prediction, a residual error is inevitably introduced. This residual can significantly influence simulation results, introducing bias into macroscopic physical quantities and corrupting the simulation even if its mean is nominally zero, leading to inaccurate system properties and dynamics. Even seemingly benign Gaussian noise in a surrogate model, if unaddressed, can lead a Monte Carlo simulation to sample an incorrect distribution, thereby biasing the derived physical observables [11]. This work presents two primary contributions. First, we show how such bias is introduced into physical observables when Monte Carlo simulations are driven by neural network potentials, even when the surrogate model exhibits good performance on test data. Second, we propose the Penalty Ensemble Method (PEM) as a robust solution to mitigate this bias. PEM quantifies epistemic uncertainty and directly integrates this information into Monte Carlo sampling through an uncertainty-aware modification of the Metropolis acceptance rule. This modification selectively increases rejection probability in regions of high predictive uncertainty, a novel mechanism that enhances the reliability and physical consistency of simulation outcomes and prevents the sampling of unphysical states.

In the following, we approximate the action of the two-dimensional ϕ^4 model using a Residual Convolutional Neural Network (RCNN see Appendix B). This RCNN surrogate is integrated into the Metropolis-Hastings (MH) algorithm, replacing the exact analytical expression for the model’s action. The inherent approximation error of the RCNN directly influences the operation of the MH algorithm. We generate samples to compute critical physical observables, exploring both far and near-phase transition regimes. Our findings clearly demonstrate how the RCNN’s approximation error biases the sampling process, leading to significant deviations in the estimations of these physical observables compared to those obtained from conventional MH simulations. To

arXiv:2506.14594v1 [cond-mat.dis-nn] 17 Jun 2025

counteract this, our work proposes the PEM to estimate the model’s uncertainty using an ensemble technique, and subsequently diminish the introduced bias with a penalty technique incorporated into the MH algorithm.

II. METROPOLIS HASTINGS ALGORITHM

Our goal is to sample configurations of the lattice ϕ^4 model, governed by the stationary distribution:

$$p(\phi) = \frac{e^{-S[\phi]}}{Z}, \quad (1)$$

where $S[\phi]$ denotes the lattice ϕ^4 action in two dimensions, as defined in [12]:

$$S[\phi] = \sum_{x \in L} \left[- \sum_{\kappa=1}^2 \beta \phi_x \phi_{x+e_\kappa} + \phi_x^2 + g (\phi_x^2 - 1)^2 \right], \quad (2)$$

with β denoting the inverse temperature and g the coupling strength. This model exhibits a phase transition between a paramagnetic and a ferromagnetic phase at a critical point $\beta_c(g)$.

The Metropolis-Hastings (MH) algorithm constructs a Markov chain by proposing updates to the field and accepting or rejecting them based on the associated change in the action. The standard steps are as follows:

1. Randomly select a site x on the lattice.
2. Propose a local update: $\phi_x \rightarrow \phi_x + \delta\phi$, where $\delta\phi \sim \mathcal{N}(0, 1)$.
3. Compute the action difference $dS = S[\phi + \delta\phi] - S[\phi]$.
4. Accept the move with probability $p_{\text{acc}} = \min(1, e^{-dS})$; otherwise, retain the current configuration.

In our work, we aim to accelerate this process by approximating the action difference dS using a residual convolutional neural network (RCNN). However, learning dS directly is difficult, as it depends on the small and fluctuating quantity $\delta\phi$. Instead, we express dS as a sum of two terms: a gradient term linear in $\delta\phi$, and a nonlinear local term that depends only on ϕ_x :

$$dS = \delta\phi \cdot \frac{\partial S[\phi_x]}{\partial \phi_x} + (6g\phi_x^2 - 2g + 1) \delta\phi^2 + 4g\phi_x \delta\phi^3 + g \delta\phi^4. \quad (3)$$

where the gradient of the action (see Appendix C) is given by:

$$\frac{\partial S[\phi_x]}{\partial \phi_x} = -\beta \sum_{\kappa=1}^2 (\phi_{x+e_\kappa} + \phi_{x-e_\kappa}) + 2(1 - 2g)\phi_x + 4g\phi_x^3. \quad (4)$$

We train the RCNN to predict $\frac{\partial S[\phi]}{\partial \phi_x} = \partial_{\phi_x} S$, which captures both local and nearest-neighbor contributions. Our goal is to evaluate the precision of this prediction—specifically its epistemic uncertainty—and adapt the acceptance probability accordingly to incorporate this uncertainty into the Monte Carlo sampling procedure.

A. Training RCNN

To train the RCNN, we provide as input a set of independent and equilibrated configurations of the field ϕ . Each image consists of $L \times L$ real-valued components. The target output is the set of gradient components $\partial_{\phi_x} S$, which we denote as ∇S .

For the training procedure, we employ the mean squared error (MSE) loss function, which corresponds to maximizing the likelihood, so that the observed data are most probable under the assumption of Gaussian noise. This choice is naturally aligned with the assumptions underlying the penalty method that we will introduce later.

After training, the RCNN is able to predict the gradient components of new equilibrated configurations. We denote these predictions as $\partial_{\phi_x} S^{\text{RCNN}}$ and define

$$dS^{\text{RCNN}} = \delta\phi \cdot \partial_{\phi_x} S^{\text{RCNN}} + (6g\phi_x^2 - 2g + 1) \delta\phi^2 + 4g\phi_x \delta\phi^3 + g \delta\phi^4. \quad (5)$$

This prediction of the action difference allows us to perform a new Monte Carlo simulation based on the RCNN prediction and on the acceptance probability:

$$p_{\text{acc}}(dS^{\text{RCNN}}, \phi', \phi) = \min(1, e^{-dS^{\text{RCNN}}(\phi', \phi)}). \quad (6)$$

We will see that this Monte Carlo based on the RCNN model does not capture the correct macroscopic behavior of the ϕ^4 model. To measure the precision of the prediction we define the residuals as:

$$R = \nabla S^{\text{RCNN}} - \nabla S. \quad (7)$$

Our first goal is to estimate the precision of these predictions, for which we design a simple ensemble method.

B. Penalty Ensemble Method

1. Deep Ensemble

We adopt a deep ensemble approach [13, 14] to estimate the precision of the predicted gradient components using N independently trained RCNN models, resulting in N distinct predictions. The difference in the predictions stems from two main factors: their training on different datasets and the convergence of stochastic optimization algorithms to a local minimum in the model

loss. Consequently, each model provides a slightly different estimate of the gradient components:

$$\{\partial_{\phi_x} S_1^{\text{RCNN}}, \partial_{\phi_x} S_2^{\text{RCNN}}, \dots, \partial_{\phi_x} S_N^{\text{RCNN}}\}. \quad (8)$$

For a given component, we define the ensemble mean $\langle \partial_{\phi_x} S^{\text{RCNN}} \rangle_N$ as the average of the N predictions and interpret it as the ensemble's best estimate of $\partial_{\phi_x} S$. To assess the uncertainty of this estimate, we compute the empirical variance:

$$\sigma^2(\phi) = \frac{1}{N-1} \sum_{i=1}^N (\partial_{\phi_x} S_i^{\text{RCNN}} - \langle \partial_{\phi_x} S_i^{\text{RCNN}} \rangle_N)^2. \quad (9)$$

Assuming the predictions are unbiased (i.e., the residuals have zero mean) and possess finite variance, the Central Limit Theorem implies that, as $N \rightarrow \infty$, the ensemble mean converges to $\partial_{\phi_x} S$ with Gaussian fluctuations of order σ/\sqrt{N} .

2. Noise Penalty Method

The noise penalty method [11] addresses the challenge of sampling from distributions where the energy cannot be computed exactly but is estimated with noise, assumed to follow a Gaussian distribution. In such cases, the acceptance probability can be modified by including a noise penalty term to ensure that detailed balance is satisfied on average to obtain a statistically correct sampling.

In our setting, using the ensemble approach to estimate the noise of the gradient in Eq. 3, the noise penalty factor reads

$$p_{\text{acc}}^{\text{PEM}}(dS^{\text{RCNN}}, \phi', \phi) = \min \left(1, \exp \left[-dS^{\text{RCNN}}(\phi', \phi) - \frac{\sigma^2(\phi)\delta\phi^2}{2N} \right] \right). \quad (10)$$

where we use the ensemble mean, $\langle \partial_{\phi} S^{\text{RCNN}} \rangle_N$, in the computation of dS^{RCNN} , and assume Gaussian-distributed residuals. Because the variance of this Gaussian is not exactly known, we rely on the empirical estimate defined by Eq. 9. While it is possible to adjust for the uncertainty introduced by this estimation [11], we will not cover this technique here.

III. RESULTS FOR METROPOLIS HASTINGS SIMULATIONS

A. Ferromagnetic and Paramagnetic Phases

We perform Monte Carlo simulations of 48×48 configurations of the ϕ^4 model, using $g = 0.1$. For this model, the inverse critical temperature is expected at $\beta_c \simeq 0.6$. We first simulate at inverse temperature $\beta = 0.7$, corresponding to the ferromagnetic phase, and at $\beta = 0.5$, corresponding to the paramagnetic phase. Standard Monte

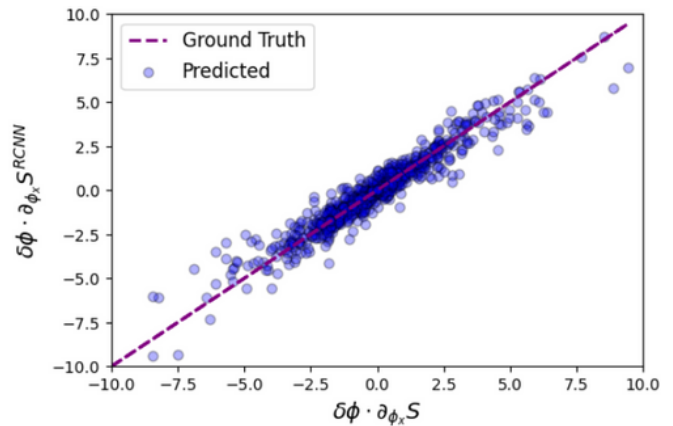


FIG. 1: Performance of the RCNN prediction.

Carlo sampling is initially performed using the exact evaluation of the gradient of the action (see Eq. 3). The data obtained from this simulation, referred to as the Ground Truth, serve as a benchmark for the data generated using the RCNN architecture, and also provide the configurations used to train the RCNN model. In all simulations we initialized the sampling with equilibrated configurations.

Then, we perform additional Monte Carlo simulations using the same parameters, but now incorporating the RCNN model predictions into the acceptance probability, as defined in Eq. (6). Each RCNN model is trained on 90 independent and equilibrated configurations previously sampled. We intentionally limit the training set size to reflect the data scarcity typically encountered in realistic physical systems. For optimization, we use the Adam algorithm, training for 150 epochs in the ferromagnetic phase and 180 epochs in the paramagnetic phase, with a batch size of 32. In Fig. 1, we assess the performance of the RCNN model by testing it on a set of configurations sampled from the ground truth algorithm. We observe that the RCNN predictions are consistently accurate across these configurations.

In Fig. 2, we present histograms of the estimated values of the action and magnetization for configurations sampled using the two different Monte Carlo methods. Although the gradient prediction errors are small, the configurations generated by the RCNN-based Monte Carlo still show significant deviations from those obtained with the ground truth method, in both the ferromagnetic and paramagnetic phases.

To correct these deviations, we implement the PEM described in the previous section. We use an ensemble of $N = 10$ independently trained models. In the Metropolis-Hastings algorithm, for each randomly selected gradient component, we compute the ensemble mean $\langle \partial_{\phi_x} S^{\text{RCNN}} \rangle_N$ and variance σ^2/N . The acceptance probability is then modified by incorporating the penalty factor, as defined in Eq. 10. Our results, shown in Fig. 2, demonstrate that the PEM successfully reproduces the

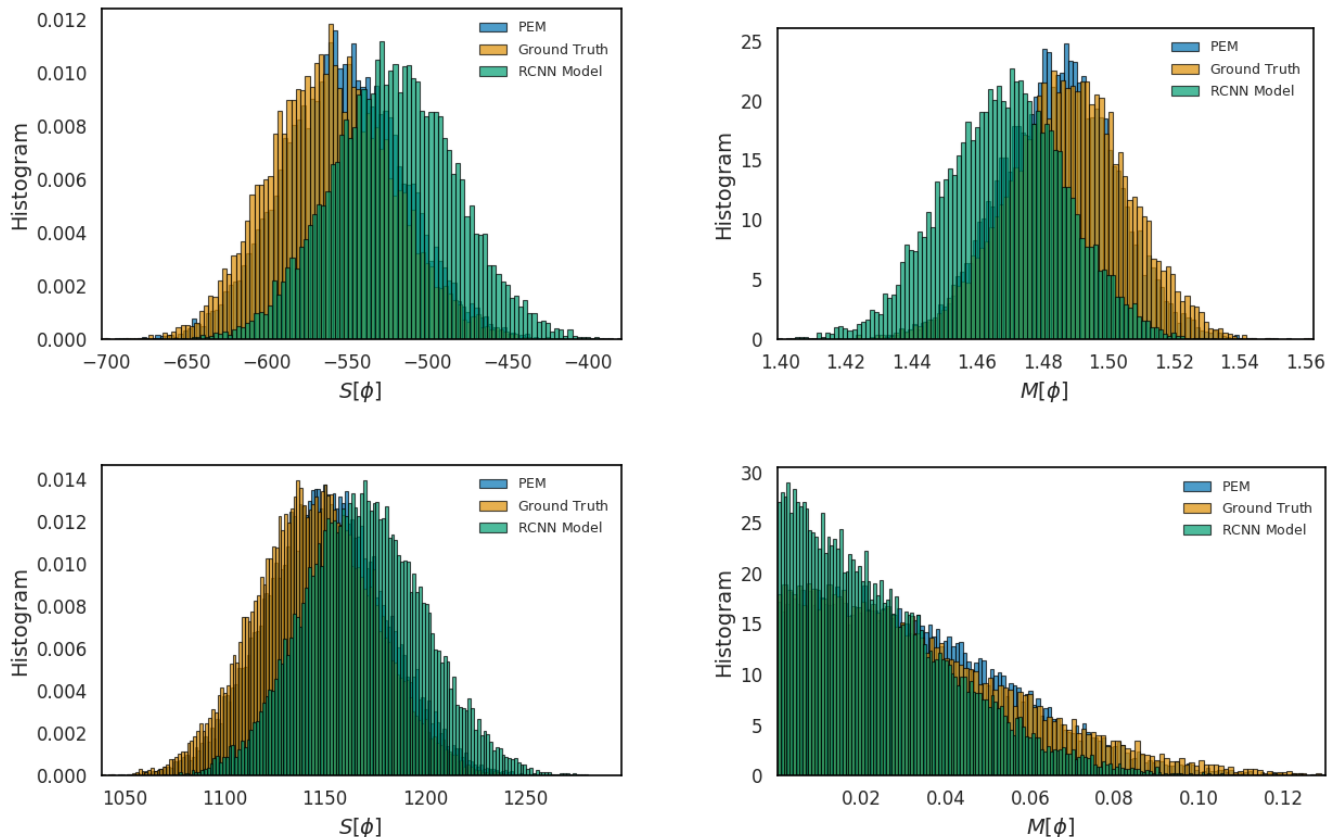


FIG. 2: Histogram of 1000 equilibrated, independent configurations of size 48×48 for the ϕ^4 model. The RCNN (green) does not sample the correct configurations, while the PEM (blue) corrects the bias. Upper panels: Ferromagnetic Phase for $\beta = 0.7$. Lower panels: Paramagnetic Phase for $\beta = 0.5$.

ground truth distributions.

B. Close to Criticality

We repeat this study near the transition point by sampling equilibrated, independent configurations at the inverse temperature $\beta = 0.6$, which we estimate to be close to criticality. Near the critical region, fluctuations become stronger and longer-ranged. To address this, we increase the RCNN training set size by a factor of 10 and perform gradient descent for 200 epochs with a batch size of 32.

In Fig. 3, we observe that the Metropolis-Hastings algorithm using only the RCNN model tends to sample configurations biased toward the paramagnetic phase. Specifically, the magnetization histogram peaks around zero. A possible explanation for this behavior is that the residual errors of the RCNN act as disorder that pushes the system toward the paramagnetic phase.

Next, we apply the PEM to sample configurations from the critical region. The results demonstrate that the PEM successfully corrects the RCNN errors, even at the critical point.

C. Non Gaussian tail in the Residual distribution

The final part of this work is dedicated to verifying the applicability of the penalty method. Specifically, we test the assumption that the residuals of the gradient components can be modeled as Gaussian random variables with zero mean and standard deviation σ . In Fig. 4, we show histograms of the residuals for both the ferromagnetic and paramagnetic phases. On a semilog scale, the bulk of the distribution closely follows a Gaussian profile, supporting the applicability of the penalty method. However, deviations from Gaussianity appear in the tails below approximately $\sim 10^{-2}$. Notably, a left-sided exponential tail is observed at the ferromagnetic point, while a symmetric exponential tail emerges at the paramagnetic point. These discrepancies likely stem from the RCNN's limited capacity to generalize in sparsely sampled regions of configuration space, where rare force configurations occur. Further details on this effect can be found in Appendix D.

To better understand the RCNN's limitations in underrepresented regions, we conduct the following experiment. We first identify a configuration in the ferromagnetic phase containing an atypical gradient component

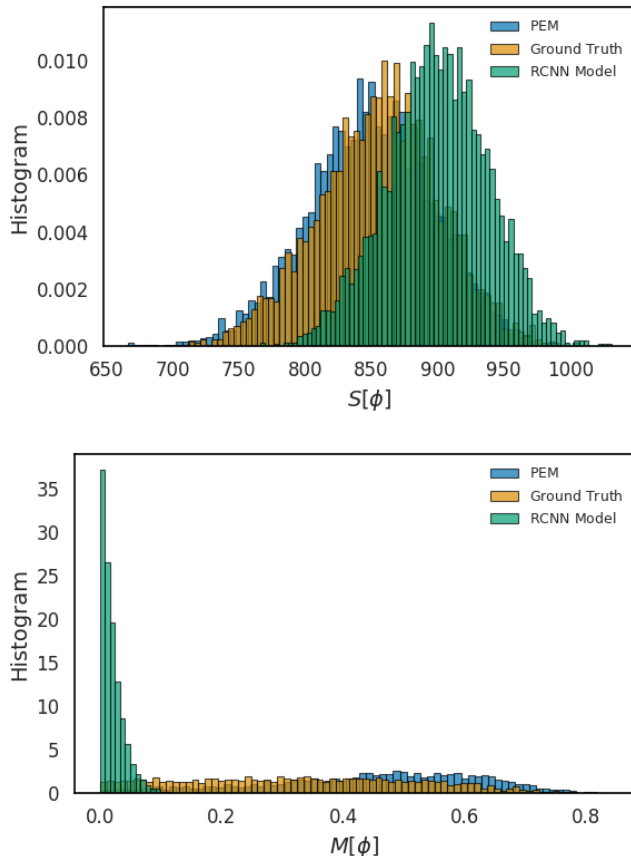


FIG. 3: Histograms of 500 equilibrated, independent configurations of size 48×48 at the critical point $\beta_c = 0.6$ for the ϕ^4 model. The RCNN (green) samples paramagnetic configurations, while the PEM (blue) recovers the correct behavior of the critical point

with a high-magnitude value (specifically, $\partial_{\phi_x} S = 8.2$). An ensemble of 1,000 RCNN models is then trained, and we collect their predictions for this specific component. For comparison, we select a typical component ($\partial_{\phi_x} S = 0.6$) and evaluate its predictions using the same trained models. The resulting residual histograms are shown in Figure 5. They reveal that predictions for the typical component closely follow a Gaussian distribution, whereas the residuals for the rare force configurations are clearly biased and exhibit heavier tails, indicating the model’s difficulty in capturing rare force configurations accurately.

As further confirmation, Figure 6 illustrates the mean and standard deviation of residuals as a function of the corresponding true gradient component, providing insight into the bias-variance behavior across the distribution.

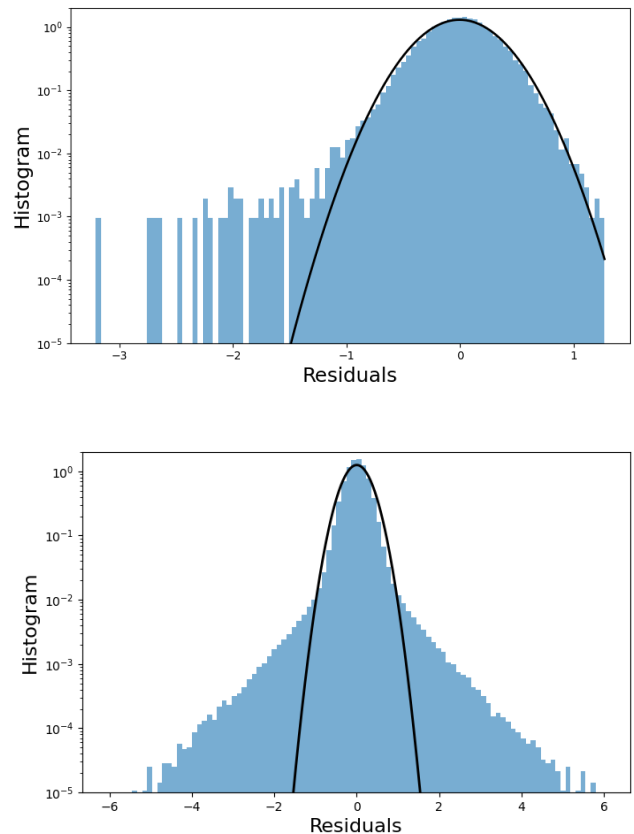


FIG. 4: Histogram of the residuals. Upper panel: Ferromagnetic phase $\beta = 0.7$. Solid black line is the Gaussian fit with $\mu = 1 \times 10^{-3}$ and $\sigma = 0.3$. Lower panel: Paramagnetic phase $\beta = 0.5$. Solid black line is the Gaussian fit with $\mu = 0.0012$ and $\sigma = 0.3$

IV. CONCLUSION

In this work, we explored the use of RCNN-based gradient estimators in Monte Carlo sampling. The predictive noise inherent to the RCNN naturally introduces stochasticity, embedding a form of epistemic uncertainty into the sampling dynamics. To better quantify and control this effect, we developed a deep ensemble method to empirically estimate the epistemic variance, which we incorporated into a modified Metropolis acceptance rule under the assumption of Gaussian-distributed predictions. This penalty-based correction improves the sampling quality by discouraging out-of-distribution proposals.

Our analysis shows that the Penalty Ensemble Method remains effective even in regimes where residuals display heavy-tailed behavior, confirming its robustness. Nevertheless, these deviations point to possible refinements, such as adaptive error bars or improved uncertainty quantification techniques. Instead of the standard MSE loss function, a more physically informed loss function might help to mitigate this effect. Finally, the penalty

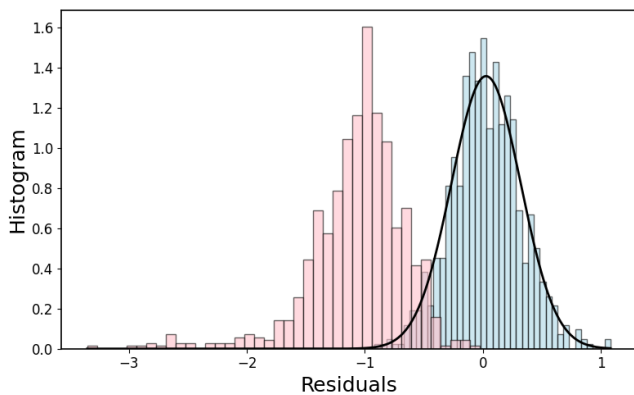


FIG. 5: Histogram of residuals for a given configuration and gradient component. The configuration is equilibrated in the ferromagnetic phase and the histogram is derived from 800 independently trained models. The light blue histogram represents a typical gradient value ($\partial_{\phi_x} S = 0.6$). Solid black line represents the Gaussian fit with $\mu = 0.027$ and $\sigma = 0.3$. The pink histogram represents an atypical gradient value ($\partial_{\phi_x} S = 8.2$).

mechanism we introduced can be naturally extended to more general sampling schemes, such as Langevin or Smart Monte Carlo [15], opening up further applications in molecular simulation.

Acknowledgments. We thank Markus Holzmann for seminal discussions and Élinor Berger for useful com-

ments.

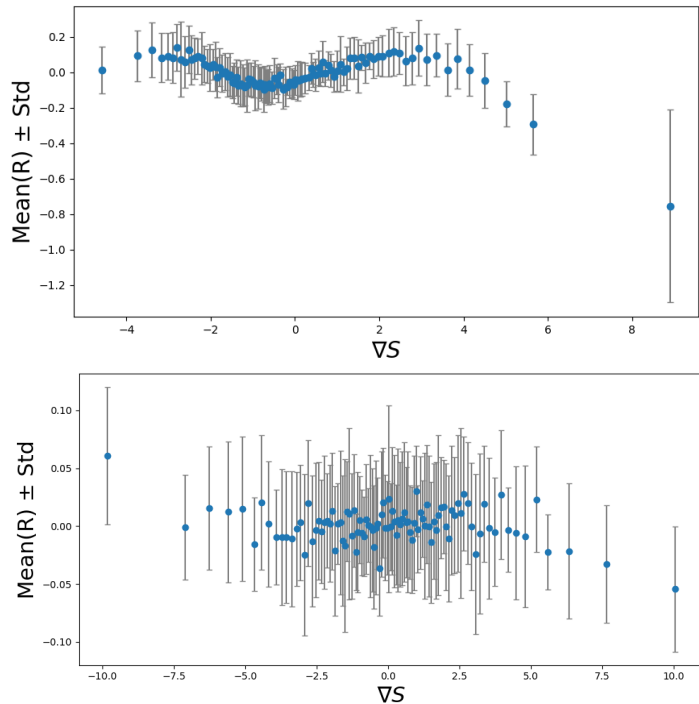


FIG. 6: Mean value and standard deviation of the residuals as a function of the ∇S . Upper panel: Ferromagnetic phase. Lower panel: Paramagnetic.

-
- [1] G. Carleo, I. Cirac, K. Cranmer, L. Daudet, M. Schuld, N. Tishby, L. Vogt-Maranto, and L. Zdeborová, *Reviews of Modern Physics* **91**, 045002 (2019).
- [2] T. T. Duignan, *ACS Physical Chemistry Au* **4**, 232 (2024).
- [3] X. Zhou, H. Liu, F. Pourpanah, T. Zeng, and X. Wang, *Neurocomputing* **489**, 449 (2022).
- [4] E. Paquet and H. L. Viktor, *BioMed Research International* **2015**, 10.1155/2015/183918 (2015).
- [5] L. M. D. Bono, F. Ricci-Tersenghi, and F. Zamponi, On the performance of machine-learning-assisted Monte Carlo in sampling from simple statistical physics models (2025), arXiv:2505.22598.
- [6] F. Noé, A. Tkatchenko, K.-R. Müller, and C. Clementi, *Annual Review of Physical Chemistry* **71**, 361 (2020).
- [7] Q. Lin, L. Zhang, Y. Zhang, and B. Jiang, *Journal of Chemical Theory and Computation* **17**, 2691 (2021).
- [8] T. D. Swinburne and D. Perez, *Machine Learning: Science and Technology* **6**, 015008 (2025).
- [9] X. Fu, Z. Wu, W. Wang, and T. Xie, in *NeurIPS 2022 Workshop AI4Science*.
- [10] B. Focassio, L. P. M. Freitas, and G. R. Schleder, *ACS Applied Materials & Interfaces* **17**, 13111 (2025).
- [11] D. M. Ceperley and M. Dewing, *The Journal of Chemical Physics* **110**, 9812–9820 (1999).
- [12] L. Del Debbio, J. Marsh Rossney, and M. Wilson, *Phys. Rev. D* **104**, 094507 (2021).
- [13] T. Garipov, P. Izmailov, D. Podoprikin, D. P. Vetrov, and A. G. Wilson, in *Advances in Neural Information Processing Systems*, Vol. 31, edited by S. Bengio, H. Wallach, H. Larochelle, K. Grauman, N. Cesa-Bianchi, and R. Garnett (Curran Associates, Inc., 2018).
- [14] B. Lakshminarayanan, A. Pritzel, and C. Blundell, in *Advances in Neural Information Processing Systems*, Vol. 30, edited by I. Guyon, U. V. Luxburg, S. Bengio, H. Wallach, R. Fergus, S. Vishwanathan, and R. Garnett (Curran Associates, Inc., 2017).
- [15] P. J. Rossky, J. D. Doll, and H. L. Friedman, *The Journal of Chemical Physics* **69**, 4628 (1978).

Appendix A: Derivation of the Noise Penalty Method

In this section, we provide the derivation of the noise penalty method as given by Ceperley and Dewing [11]. Note that in the original derivation, it is assumed that

when a move from ϕ to ϕ' is proposed, the estimate of the energy difference has a Gaussian error with zero mean and standard deviation σ , independent of ϕ and ϕ' . Actually, the same result holds for a more general case where $\sigma = \sigma(\phi, \phi')$. In our implementation, we estimate the standard deviation empirically, and it depends on ϕ .

Our goal is to derive the modified acceptance probability $p_{\text{acc}}(dS^{\text{RCNN}}, \phi, \phi')$, based on the RCNN estimate dS^{RCNN} of the true energy difference dS . This probability must satisfy the detailed balance condition **on average**:

$$\langle p_{\text{acc}}(dS^{\text{RCNN}}, \phi, \phi') \rangle = e^{-dS} \langle p_{\text{acc}}(dS^{\text{RCNN}}, \phi', \phi) \rangle. \quad (\text{A1})$$

Here, the ensemble average $\langle \dots \rangle$ is taken over all possible estimates dS^{RCNN} . We assume that these estimates have Gaussian fluctuations around the true value dS , namely:

$$dS^{\text{RCNN}} = dS + \sigma(\phi, \phi')\epsilon, \quad (\text{A2})$$

where ϵ is a normally distributed random variable. The solution

$$p_{\text{acc}}(dS^{\text{RCNN}}, \phi, \phi') = \min \left\{ 1, \exp \left[-dS^{\text{RCNN}} - \frac{1}{2}\sigma^2(\phi, \phi') \right] \right\}. \quad (\text{A3})$$

should be averaged over all possible estimates dS^{RCNN} assuming Eq. A2. It is then possible to verify that this solution ensures in average the detailed balance of Eq. A1.

Appendix B: Residual Convolutional Neural Networks approximation

To approximate the ∇S in ϕ^4 field theory, Convolutional Neural Networks (CNNs) offer an effective solution for regression tasks. A key advantage of CNNs in lattice field theory lies in their ability to naturally capture and preserve translational invariance, a fundamental symmetry of the system. An important technical consideration is the use of periodic boundary conditions (PBC) during the training of the neural network. These are implemented through periodic padding in the RCNN architecture, ensuring consistent interactions between neighboring lattice sites, even across boundaries. In contrast, simple neural networks often exhibit strong bias, leading to poor predictive performance. Our neural network

architecture, detailed in Fig.7, consists of an initial convolutional layer, followed by Batch Normalization and a ReLU activation function. This is followed by a residual block, which includes another convolutional layer, batch normalization, and ReLU activation. A projection layer is introduced to align the residual connection, ensuring compatibility in feature dimensions. The output of the residual block is summed with the projected residual connection before passing through a final convolutional layer to generate the output. The inclusion of a residual connection allows the model to bypass certain transformations, mitigating the vanishing gradient problem and facilitating more efficient feature propagation. This enables deeper feature extraction while preserving relevant information from earlier layers.

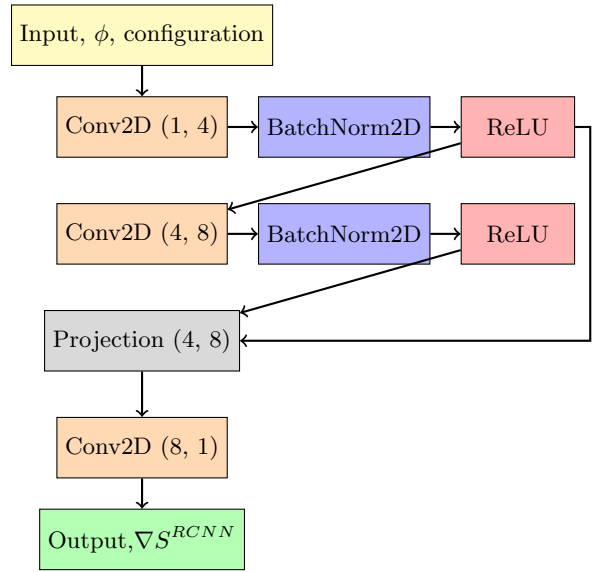


FIG. 7: Fully Convolutional Residual CNN Architecture

Appendix C: Gradient of Action

The gradient of the action for the ϕ^4 model is the following:

$$\begin{aligned} \frac{d S[\phi_{ij}]}{d\phi_{km}} &= \frac{d}{d\phi_{km}} \left[-\beta \sum_{ij}^L \phi_{ij} (\phi_{i+1,j} + \phi_{i,j+1}) + \phi_{ij}^2 + g(\phi_{ij}^2 - 1)^2 \right] = \\ &= -\beta \sum_{ij}^L \delta_{ik} \delta_{jm} (\phi_{i+1,j} + \phi_{i,j+1}) + \phi_{ij} (\delta_{i+1,k} \delta_{jm} + \delta_{ik} \delta_{j+1,m}) + 2\delta_{ik} \delta_{jm} \phi_{ij} + 4g\delta_{ik} \delta_{jm} \phi_{ij} (\phi_{ij}^2 - 1) \Rightarrow \\ \frac{d}{d\phi_{km}} S[\phi_{ij}] &= -\beta (\phi_{k+1,m} + \phi_{k-1,m} + \phi_{km+1} + \phi_{km-1}) + 2\phi_{km} + 4g\phi_{km} (\phi_{km}^2 - 1). \end{aligned} \quad (\text{C1})$$

Appendix D: Histograms of the gradients.

In Fig. 8 and 9, we compare histograms of the true gradient components with those predicted by the RCNN. The RCNN fails to reproduce the exponential tails corresponding to large or very small gradient values, indicating an inability to capture the full support of the target gradient field.

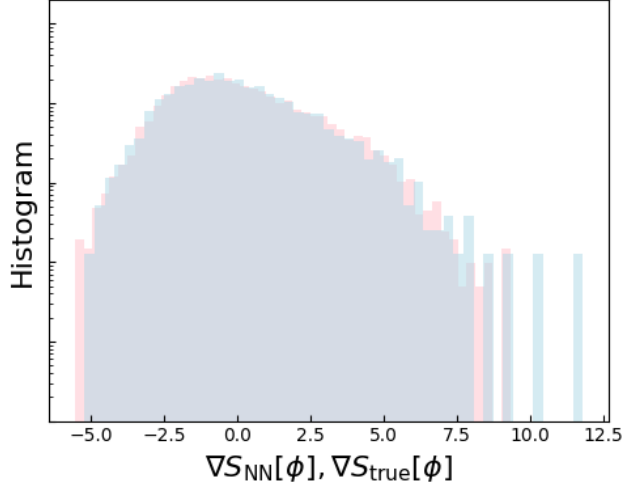


FIG. 8: Histogram in lin-log scale of the true gradients (light blue) vs the RCNN predicted gradients (pink) in the Ferromagnetic phase.

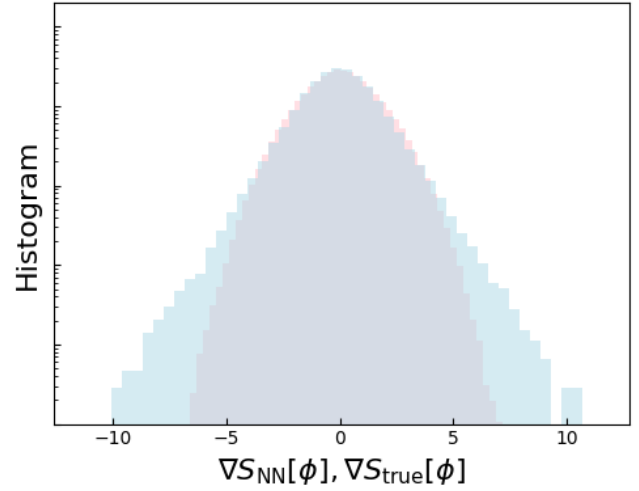


FIG. 9: Histogram in lin-log scale of the true gradients (light blue) vs the RCNN predicted gradients (pink) in the Paramagnetic phase.